Modeling of MIG/MAG Welding with Experimental Validation using an Active Contour Algorithm applied on High Speed Movies

Jean-Pierre Planckaert [a,b], El-Hadi Djermoune [a,*], David Brie [a], Francis Briand [b] and Frédéric Richard [b]

[a] *Centre de Recherche en Automatique de Nancy, Nancy-Université, CNRS*
Boulevard des Aiguillettes, B.P. 239, 54506 Vandoeuvre-lès-Nancy Cedex, France

[b] *Air Liquide–CTAS*
13 rue des Epluches, St-Ouen l'Aumône, 95315 Cergy-Pontoise Cedex, France

Abstract

This paper investigates some issues in physical modeling of metal inert gas/metal active gas (MIG/MAG) welding process in the short arc mode. In this mode, a metal supply is molten in the arc state and then transferred to the weld pool during the short-circuit state. A hybrid model having two distinct continuous states whose switchings are controlled by two guard conditions is proposed. Due to the complexity of the physical phenomena involved in the welding process, simplifications are used to obtain a model accounting for the main physical contributions but simple enough to yield an efficient, fast and numerically tractable simulator which can be used intensively for evaluating different control strategies. In an attempt to validate the proposed model, different measurements have been made including supply

voltage and current sampled synchronously with high speed digital video. In order to extract some relevant quantities representative of the metal transfer from image sequences, an active contour algorithm is developed and tested. The effectiveness of the proposed model in the prediction of major tendencies of a welding process, especially in the arc state, is shown using experimental data. Some limitations of the model during the metal transfer are also stressed and possible remedies are then proposed.

Key words: MIG/MAG welding, physical modeling, dynamic active contour
PACS:

1 Introduction

The metal inert gas/metal active gas (MIG/MAG) welding is an arc welding process in which additional metal is brought by a roll of wire line and is molten by Joule effect and an electric arc [1]. In the short arc mode, the weld is made by successive drops. An inert gas, generally argon based gas (MIG welding), or active gas, generally CO_2 based gas (MAG welding) is used as plasma for electric arc outbreak and as protective atmosphere for metal at high temperature, avoiding contamination of the metal by oxygen and nitrogen. The welding generator supplies the electric energy required for melting and

* Corresponding author.
Email addresses: jean-pierre.planckaert@airliquide.com (Jean-Pierre Planckaert), el-hadi.djermoune@cran.uhp-nancy.fr (El-Hadi Djermoune), david.brie@cran.uhp-nancy.fr (David Brie), francis.briand@airliquide.com (Francis Briand), frederic-p.richard@airliquide.com (Frédéric Richard).

for arc outbreak and sustainment between wire and workpieces to weld. It works according to two distinct control modes: 1) the arc mode in which the voltage delivered by the generator is controlled to reach a set point chosen by the welder; 2) the short circuit mode in which the current follows a pre-defined law.

The general framework of this study concerns the modeling of the MIG/MAG welding process for a metal transfer in short arc mode. It aims at providing a model of the whole system including wire, gas, arc, sheet metal and control. Not only such a model is expected to give some insights into the understanding of the welding process but its implementation in the simulator is intended to assess the effectiveness of different control strategies as well as the effects the experimental setup on the control performances. Hence, the model should be precise enough to produce the major tendencies but simple enough to result in a fast simulator which can be used intensively.

The molten metal drop detachment from an electrode in gas metal arc welding involves complex interactions between different physical phenomena. Some authors have studied the electromagnetic effects [2–5], and others the thermal effects [6] and the fluid dynamics [7]. As a consequence, sophisticated mathematical models have been developed, including arc plasma generation, electrode melting, droplet formation, detachment and impingement onto the base metal. Generally speaking, the most used numerical techniques belong to the class of Eulerian methods such as volume of fluid or level set methods. These methods enable one to take into account all physical phenomena with limited assumptions on the droplet shape, stream lines, etc. For instance, Choi *et al.* used the volume of fluid to simulate the spray and globular metal transfer modes [7], as well as the short-circuit mode [8]. The model have been extended

by Zhu *et al.* [9], in the spray and globular modes, to account for the thermal phenomena in both the droplet and the molten pool. Although these models generally achieve a precise simulation of the MIG/MAG process, they suffer from some practical difficulties which are closely linked to the calculation time/precision trade-off and may suffer from instability problems. Hence, some simplified models have been also proposed assuming, for instance, a flat weld-pool surface, truncated spherical droplets, stable transfer, etc. [10–12]. These models are clearly less precise but account for the main tendencies. Inspired by these articles, we propose a hybrid model accounting for the switching from the arc mode to the short-circuit mode [13] taking into account the main forces acting on the molten metal during a complete cycle, and we validate it by comparison with experimental data. The recordings are realised on a test bed equipped with an acquisition system measuring voltage, current and wire feed speed. All these measurements are sampled synchronously with a high speed video system operating at 10000 frames per second. The video images are processed to measure some relevant quantities for model validation, such as molten metal bridge volume, bridge minimal diameter or surface of contact between bridge and weld pool. In that respect, it is necessary to perform a segmentation of the images. However our images are too complex to expect local, low level operations to generate perfect primitives. Higher level features have to be used to get a better delineation of objects. So, we chose to use deformable models which adapt to the data, which is the case of active contour algorithms [14]. This step enables one to measure indirectly the geometry of the drops that is inaccessible by the acquisition system. The obtained variables are used here to validate the proposed model, but they may be also exploited to build a database from which model identification, with physical prior, can be achieved.

The paper is organised as follows. In Section 2, a description of the physical aspect of Gas Metal Arc Welding (GMAW) in the short arc mode is given. After having introduced the main forces acting in the process, we chose the variables of interest in order to implement a model of the system. Next, in Section 3, we introduce the active contour methodology allowing us to observe these variables. Experimental results are given in Section 4. They show the approach effectiveness (as well as its limitation) to give access to the dynamic of the chosen variables. Finally, the conclusion raises some issues to be developed in future work.

2 GMAW System in Short Arc Mode

2.1 General Description

Short-circuiting metal transfer is a metal transfer whereby a continuously fed wire electrode is deposited during electrical short-circuits. The transfer of a single molten droplet of electrode occurs during the shorting phase of the transfer cycle when physical contact with the molten weld pool occurs.

Fig. 1 illustrates the time evolution of a droplet together with the corresponding arc voltage and welding current. Metal transfer goes through five steps:

- A: The electrode makes physical contact with the molten pool. The arc voltage approaches zero and the current level increases. The rate of rise to the peak current is affected by the amount of applied inductance.
- B: This point demonstrates the effect of electromagnetic forces that are applied around the electrode. This force pinches the electrode.

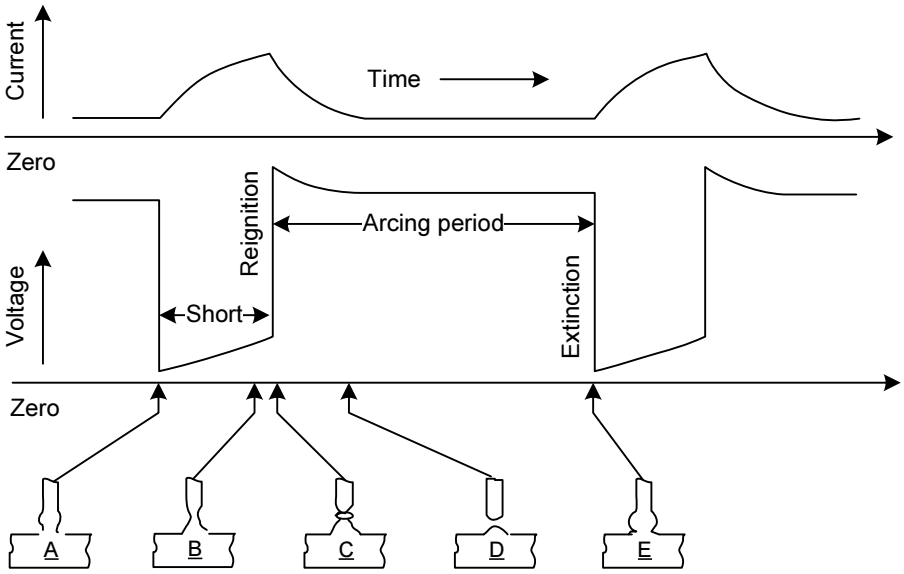

Fig. 1. Oscillograms and sketches of short circuiting transfer.

- C: This is the point where the bridge of molten metal explodes. The droplet is forced from the tip of the electrode to the welding pool.
- D: The molten droplet reforms while current is at its background level.
- E: The electrode is once again making contact with the pool, preparing for the transfer of another droplet.

The area of the welding arc, sketched on Fig. 2, is a region of high complexity that is comprised of physical forces and chemical reactions. The interaction of the components of the arc affects metal transfer and the quality of the finished weld. The behavior of the arc is influenced by: the type and the diameter of the filler metal, the base metal conditions, the shielding gas, the welding parameters (voltage and current) and the interaction of physical forces.

The phenomenon of metal transfer in short arc welding can be seen as a hybrid system as sketched on Fig. 3. Indeed it presents two continuous states: a first one during which the droplet grows and a second one during which the electrode is in physical contact with the workpiece. The jump between the two

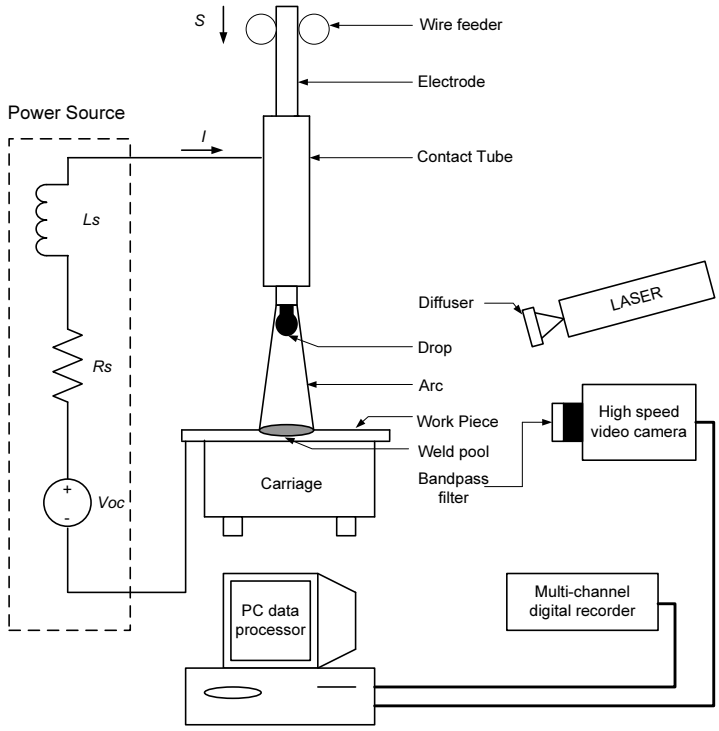

Fig. 2. Sketch of the experimental apparatus.

states is linked to the fulfillment of a guard condition:

- Cond 1: The contact-tube to workpiece distance is less than the electrode extension plus droplet length,
- Cond 2: the molten metal bridge diameter is less than a threshold fixed by electrical and material laws.

In each state, a set of differential equations drives the process behaviour. These equations stem from power source characteristics, the set of forces acting on a droplet and fluid dynamics for the metal transfer.

2.2 Model of Droplet Growth

Two categories of forces can arise in our process: detaching ones and retaining ones. Three forces have been identified as relevant:

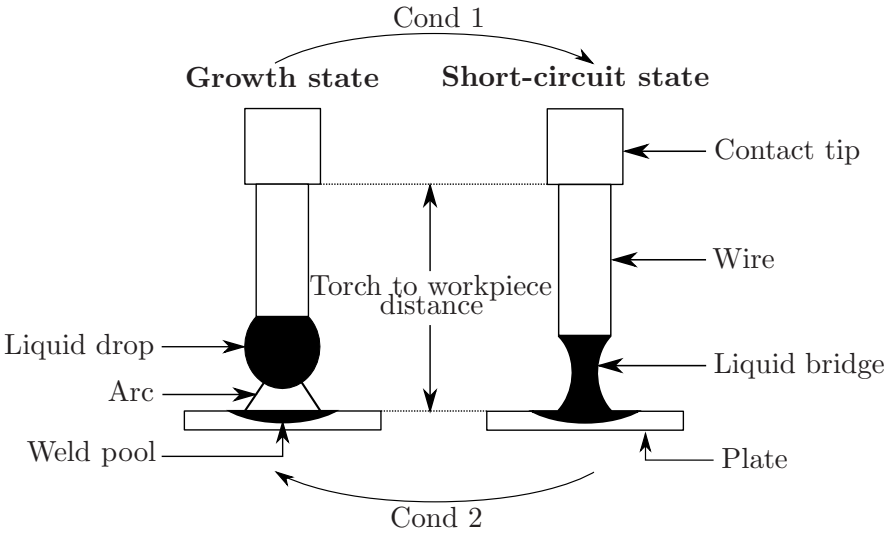

Fig. 3. States of the hybrid system.

(1) The gravitational force due to the mass of the drop and acts as a detaching force when welding in the flat position:

$$F_g = \frac{4}{3}\pi r_d^3 \rho_w g \tag{1}$$

where r_d denotes the droplet radius, ρ_w the mass density of molten metal, and g the gravity acceleration.

(2) The surface tension is a property of all liquids which comes from the surface of a liquid has an energy (more precisely the interface between the liquid and the phase surrounding it). This energy is reduced by minimizing the area for any volume. This is realized when the liquid takes a spherical shape as the ratio area/volume is minimal for a sphere. In 1864, Tate observed the direct proportionality between the maximum mass of a drop of water detached from a pipe and the radius of the pipe. This relation is known as Tate's law and is given by:

$$F_S = 2\pi r_w \gamma \tag{2}$$

with F_S the weight of the drop, r_w the radius of the tip (in MIG/MAG

welding, the radius of the electrode) and γ the liquid surface tension. In their study of 1919 Harkins and Brown [15] proposed a modification of (2) based on the observation that with each drop forming at the end of the tip, all of the liquid does not detach and some remains on the tip. Defining F'_S as the weight of liquid actually detached from the tip, (2) becomes:

$$F'_S = 2\pi r_w \gamma f \tag{3}$$

where f is an empirical correction function which will take the unity value for an ideal drop detaching totally from the pipe.

(3) The electromagnetic force which results from diverging or converging current flow within the electrode. As shown on Fig. 5, if the current lines diverge in the drop, the Lorentz force, which acts at right angle to these current lines, creates a detaching force; on the contrary, if the current lines converge, the Lorentz force opposes drop detachment. This force is calculated thanks to the Lorentz's law:

$$\overrightarrow{F}_{em} = \overrightarrow{J} \times \overrightarrow{B} \tag{4}$$

where $\overrightarrow{J}$ is the current density and $\overrightarrow{B}$ the magnetic flux. The total electromagnetic force can be obtained by integrating (4) over the current conducting surface of the drop. By assuming that the current density on the drop is uniform, Amson [5] obtained:

$$F_{emz} = \frac{\mu_0 I^2}{4\pi} f_z \tag{5}$$

and

$$f_z = -\left[\frac{1}{4} - \ln\left(\frac{r_d \sin\theta}{r_w}\right) + \frac{1}{1-\cos\theta} - \frac{2}{(1-\cos\theta)^2} \ln\left(\frac{2}{1+\cos\theta}\right)\right] \tag{6}$$

where I is the welding current and μ_0 is the permeability of free space. The geometry used in (6) is shown on Fig. 4 where θ is the arc hanging angle. The black surface indicates the area of the drop allowing the current to go through the plasma (this area is called the anode spot). A graph of f_z as a function of the conduction zone angle is given in Fig. 6. As it can be seen on Fig. 5, when the conduction zone is small such that the current lines converge (the current lines are included between the dotted lines), f_z becomes negative so the electromagnetic force acts as a repulsive force. When the conduction zone is large enough so that the current lines diverge, f_z becomes positive and the electromagnetic force becomes a detaching force.

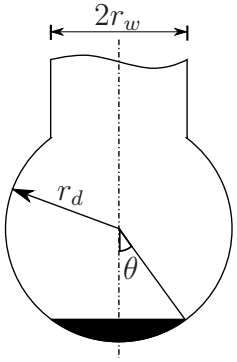

Fig. 4. Geometry of a drop.

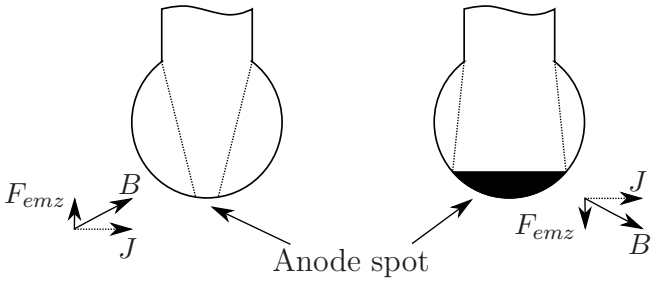

Fig. 5. Current path and Lorentz force.

In MIG/MAG welding metal, transfer only occurs after the solid is molten and thus the coupling between mass flow and heat transfer is very strong. The main heat sources for melting the electrode are Joule effect and electron

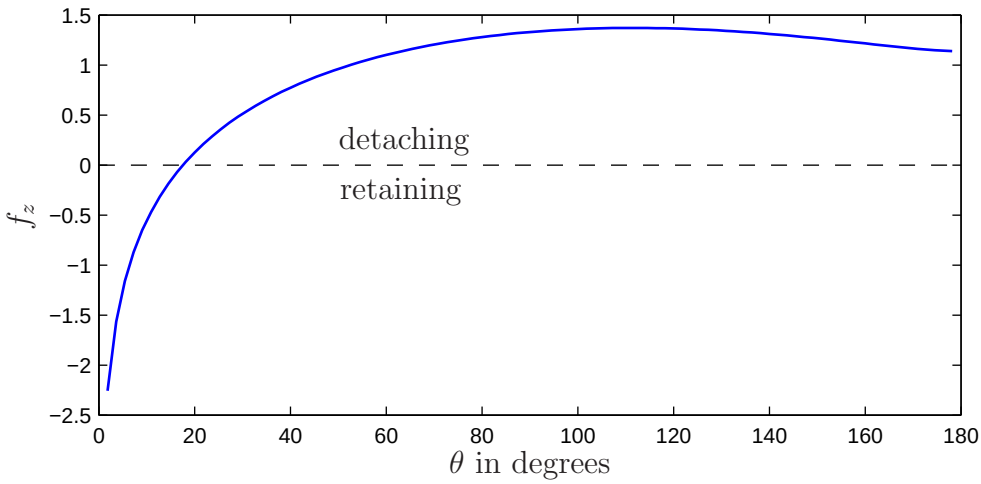

Fig. 6. Variation of f_z as a function of θ.

condensation [16]. Joule heat is the heat generated by the electrical resistance of the consumable electrode. The heat of electrode condensation results from the plasma high energy electrons condensing on the metal surface and releasing most of their energy.

The Joule heat can be calculated by:

$$Q_{joule} = \int_V \rho(T) I^2 dV = \overline{\rho} A L I^2 \tag{7}$$

where $\overline{\rho}$ is the average electrical resistivity, L the electrode extension and A the area of the electrode. The electrode condensation heat can be obtained by:

$$Q_{cond} = \left(\frac{3}{2} \frac{kT}{e} + V_a + \Phi \right) I \tag{8}$$

with k denotes the Boltzmann constant. The first term of the right hand-side of (8) represents the kinetic energy of the electrons in the plasma, the second term is the acceleration energy of the electrons in the anode drop region and the third term is the work function of the electrode material.

If one assumes that the whole heat is consumed in melting the consumable electrode, the melting rate can be obtained by dividing the total heat input into the system by the heat required to melt a unit mass of the material:

$$\frac{dm}{dt} = \frac{\overline{\rho} A L I^2 + \left(\frac{3}{2}\frac{kT}{e} + V_a + \Phi\right) I}{\int_{T_i}^{T_m} C_p dT + \Delta H_{trans} + \Delta H_m} \tag{9}$$

where ΔH_{tans} is the heat of cristalline transition and ΔH_m is the heat of fusion. Since the coefficients are constant the melting rate can be expressed as a second order function of the welding current:

$$\frac{dm}{dt} = (C_1 I + C_2 \rho l_s I^2)\rho_w \tag{10}$$

where C_1 and C_2 are constant parameters fixed to strike a balance between Joule effect and arc heat fusions, $\rho = \bar{\rho} A$ denotes the linear resistivity of the electrode and l_s represents the solid wire extension (stick-out).

The power supply being converted into the equivalent RL circuit [12], we write the Kirchoff's voltage law for the welding system represented on Fig. 2 as:

$$L_S \frac{dI}{dt} + (R_S + R)I + U_{arc} = U_{oc} \tag{11}$$

with L_S and R_S are the inductance and resistance of the welding system, R is the wire-droplet system resistance, U_{oc} is the equivalent open-circuit voltage and U_{arc} is the arc voltage. The latter is expressed by:

$$U_{arc} = U_0 + R_a I + E_a(CT - l_s) \tag{12}$$

where U_0 is the arc voltage constant, E_a the arc length factor, CT the contact tube to workpiece distance and R_a the arc resistance.

The stick-out evolution is controlled by:

$$\frac{dl_s}{dt} = S - \frac{1}{\pi r_w^2}\frac{dm}{dt} \tag{13}$$

with S the wire feed speed.

We have used these expressions of forces, of melting rate and of evolution of the welding current to write a state-space representation of the governing differential equations of droplet growth. Five state variables have been retained: droplet displacement x_1, droplet velocity x_2, current x_3, stick-out x_4 and droplet mass x_5. State equations are:

$$\dot{x}_1 = x_2 \tag{14}$$

$$\dot{x}_2 = \frac{1}{x_5}(F_g + F_{em} - F_S) \tag{15}$$

$$\dot{x}_3 = \frac{1}{L_S}\left[U_{oc} - (R_a + R_S)x_3 - U_0 - E_a(CT - x_4) - \left[x_4 + x_1 + \left(\frac{3x_5}{4\pi\rho_w}\right)^{\frac{1}{3}}\right]\rho x_3\right] \tag{16}$$

$$\dot{x}_4 = S - \frac{1}{\pi r_w^2}(C_1 x_3 + C_2 \rho x_3^2 x_4) \tag{17}$$

$$\dot{x}_5 = (C_1 x_3 + C_2 \rho x_3^2 x_4)\rho_w \tag{18}$$

In order to implement the model of the system shown on Fig. 3, offering a good agreement with the practical work of the process, it is necessary to supervise some variables of interest during a normal operation of the testing bed. Indeed, we need the dynamic behaviour of the volume of the drop, the center of gravity and the liquid-solid border synchronously with arc voltage and welding current. So an experimental database has been built with electrical measurements and high speed videos. The work presented in Section 3 aims at extracting information concerning the droplet from videos. In this purpose we decided to use active contours.

2.3 Model of Metal Transfer

We present here a simple model of metal transfer during short-circuiting period. Through this work we aim at checking some ideas often encountered when dealing with welding.

The power supply being converted into the equivalent RL circuit [12], we write the Kirchoff's voltage law for the welding system represented on Fig. 2 as:

$$L_S \frac{dI}{dt} + (R_S + R)I = U_{oc} \tag{19}$$

The metal transfer is controlled by three relevant forces:

(1) The gravitational force.

(2) The electromagnetic force which results from diverging or converging current flow within the electrode. When the current path diverges in the drop, the Lorentz force presents an axial component acting, normal to the current path and creating a detaching force, and an orthoradial component which squeezes the molten metal bridge.

(3) The surface tension which is normal to the surface of a molten droplet. It serves to support the form of the molten metal bridge.

An exhaustive welding simulation would solve a set of coupled partial differential equations governing the fluid, thermal and electromagnetic fields. These equations would include the continuity and Navier-Stokes equations. The following assumptions [11] are made to simplify the complex behavior of short circuiting transfer:

(1) The initial bridge shape is spherical and the contact diameter within the weld pool surface is equal to the wire diameter.

(2) Flow velocity within the bridge and pressure within the weld pool are neglected.

(3) The bridge shape is described by two principal radii.

(4) The pool surface remains flat and metal transfer is stable.

Thanks to these assumptions and taking into account only the three forces mentioned above we expect to model the sequence of events represented on Fig. 7.

The average pressure on the cross section of the bridge center with a configuration of principal radii as in Fig. 8 is [11]:

$$P_{avg} = \frac{\mu_0 I^2}{8\pi^2 R_1^2} + \gamma\left(\frac{1}{R_1} + \frac{1}{R_2}\right) \tag{20}$$

Applying the Bernoulli equation with assumption 2, the flow velocity at the contact between the bridge and pool surface can be calculated using the average pressure and bridge height as:

$$v = \sqrt{\frac{2}{\rho_w}(P_{avg} + \rho_w g h)} \tag{21}$$

where h is the distance between the pool surface and bridge center. Finally, the state-space model corresponding to the metal transfer mode is given by:

$$\dot{x}_1 = x_2 \tag{22}$$

$$\dot{x}_2 = \frac{1}{x_5}(F_g + F_{em} - F_S) \tag{23}$$

$$\dot{x}_3 = \frac{1}{L_S}\left[U_{oc} - R_S x_3 - \left[x_4 + x_1 + \left(\frac{3x_5}{4\pi\rho_w}\right)^{\frac{1}{3}}\right]\rho x_3\right] \tag{24}$$

$$\dot{x}_4 = S - \frac{C_2 \rho x_3^2 x_4}{\pi r_w^2} \tag{25}$$

$$\dot{x}_5 = \left(C_2 \rho x_3^2 x_4 - \sqrt{\frac{2}{\rho_w}(P_{avg} + \rho_w g h)} A_c\right)\rho_w \tag{26}$$

where A_c is the exchange surface between the liquid metal bridge and the weld

pool.

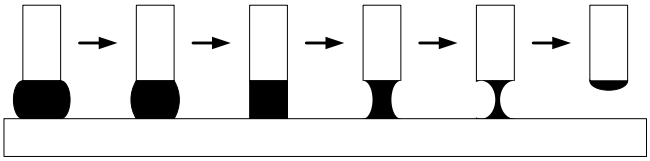

Fig. 7. Short circuit modeling.

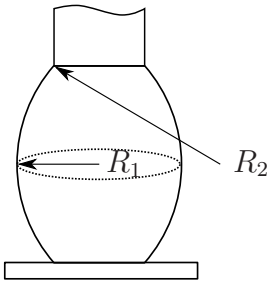

Fig. 8. Bridge configuration with principal radii.

2.4 Implementation of the Hybrid Model

The hybrid model for MIG/MAG welding has been implemented in the Matlab language. The simulation of the continuous state is performed by the Runge-Kutta solver and the main difficulty was to handle with the switching between the two continuous states. The values of the state variables obtained at the end of one continuous state are used as initial conditions for the other continuous state.

The switching from the droplet growth state to the metal transfer state is achieved when the distance between the drop and the weld pool equals zero. This consists in checking whether the sum of the stick-out l_s (state variable x_4) and the drop height, obtained thanks to its mass and geometry (truncated sphere, see Fig. 4), equals the contact tip to workpiece distance CT.

The switching from the metal transfer state to the droplet growth state is

controlled by the molten metal bridge radius (R_1). It is obtained from the volume of the bridge using once again its geometry (see Fig. 8).

3 Active Contour Segmentation

In order to implement the model of the system shown on Fig. 3, offering a good agreement with the practical work of the process, it is necessary to supervise some variables of interest during a normal operation of the testing bed. Indeed, we need the dynamic behaviour of the volume of the bridge, the minimal diameter of the bridge and the surface of contact between the bridge and the pool synchronously with arc voltage and welding current. So an experimental database has been built with electrical measurements and high speed videos. The work presented in Section 3 aims at extracting information concerning the drop from videos. In this purpose we decided to use active contours.

Contour extraction is often used in technical and scientific fields. It can be employed for shape recognition in industry applications or to process images in astronomy to make them clearer. Our study requires the use of such techniques in order to observe the dynamical behaviour of molten metal at the end of the electrode.

Standard segmentation methods can be seen as low-level methods. They offer the detection of elements in the picture. They create a division of the image in separated homogeneous regions by considering contours as places of significant variation of information. Nevertheless they do not execute the last step we need. Indeed the metrology is not allowed by these methods and we are looking for quantitative information about the drop geometry during the arc period

and about the liquid bridge shape during the short-circuit period. That is why we have chosen active contours as a high-level method performing this last step.

3.1 Theory

Active contour models introduced by Kass and Witkins [14] have rapidly seduced the scientific community by their ability to efficiently combine both the available *a priori* knowledge about the structure of interest and local correspondance with the image features [17–19]. Their principle is to evolve from an initial contour to equilibrium which corresponds to the edges of the object to detect.

Active contour models are also known as *snakes* or *minimizing curves*. This is a semi-interactive method in which the user puts an initial contour in the image (near the shape to find) and this one will be deformed by the action of several energies. The contour will evolve searching the position of lowest local energy.

In its continuous form, the snake is described by a parametric curve $v(s) = [x(s), y(s)]^t$ with $s \in [0, 1]$ and $v(0) = v(1)$ for a closed contour. Its total energy can be written as:

$$E_{snake} = \int_0^1 \Big[E_{int}(v(s)) + E_{im}(v(s)) + E_{ext}(v(s)) \Big] ds \tag{27}$$

where E_{int}, E_{im} and E_{ext} denote internal, image and external energies, respectively. The internal energy depends only on the contour shape. It is given

by:

$$E_{int}(v(s)) = \alpha E_{cont}(v(s)) + \beta E_{curv}(v(s)) \tag{28}$$

$$= \alpha \left(\frac{dv}{ds}\right)^2 + \beta \left(\frac{d^2v}{d^2s}\right)^2 \tag{29}$$

The first order term drives continuity while the second order term controls curvature.

The potential energy related to the image can be written as:

$$E_{im}(v(s)) = -\lambda(s)|\nabla I(v(s))|^2 \tag{30}$$

This energy qualifies the elements towards which we want to attract the contour on the image. In the segmentation framework it corresponds to the lines of high gradient.

The external energy is user defined in accordance with the problem specificities. For instance we can impose a minimal distance between two consecutive points of the snake. Without an external energy and when high gradient lines are sought we can write:

$$E_{snake}(v(s)) = \alpha E_{cont}(v(s)) + \beta E_{curv}(v(s)) + \sigma E_{im}(v(s)) \tag{31}$$

The triplet (α, β, σ) enables to strike a balance between different energies. In the continuous domain, the energy equation of a contour C can be expressed by:

$$E_{snake} = \int_C \left[-\sigma(s)|\nabla I(v(s))|^2 + \alpha \left(\frac{dv}{ds}\right)^2 + \beta \left(\frac{d^2v}{d^2s}\right)^2\right] ds \tag{32}$$

In a discrete approach, the contour is a list of points M_i, $i \in [1, n]$. The energy of the snake is assimilated to the sum of the energies associated to the n points defining it:

$$E_{snake} = \sum_{i=1}^{n} \Big[\alpha E_{cont}(M_i) + \beta E_{curv}(M_i) + \sigma E_{im}(M_i)\Big] \tag{33}$$

3.2 Algorithm

In order to minimize E_{snake}, we determine the list of n points constituting C. To achieve this goal we have chosen to implement the *greedy* algorithm [20–22]. In this approach the derivatives in (32) have to be approximated by finite differences. If $v_i = [x_i, y_i]^t$ is a point of the contour, we write:

$$\left|\frac{dv_i}{ds}\right|^2 \approx |v_i - v_{i-1}|^2 = (x_i - x_{i-1})^2 + (y_i - y_{i-1})^2 \tag{34}$$

and

$$\left|\frac{d^2v_i}{ds^2}\right|^2 \approx |v_{i-1} - 2v_i + v_{i+1}|^2 = (x_{i-1} - 2x_i + x_{i+1})^2 + (y_{i-1} - 2y_i + y_{i+1})^2 \tag{35}$$

Two assumptions have been made here:

- the points are spaced at unit intervals. If the points are evenly spaced, then (34) should be divided by d^2, where d is the distance between points and (35) by d^4.
- if the points are not evenly spaced, the first derivative term will be divided by d_i^2 where d_i is the distance between points i and $i-1$.

The third term in (31), E_{im}, is the image force, which is the gradient magnitude at each point in the image, intensity being coded as an eight bit integer.

The *greedy* algorithm is iterative. During each iteration, a neighborhood of each point is examined and the point in the neighborhood giving the smallest value for the energy term is chosen as the new location of the point.

Our final aim is to get information on the drop evolution. To achieve it, we have acquired a set of movies which are lists of images. Consequently, the idea

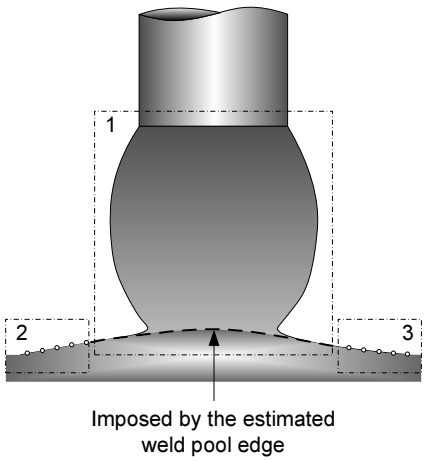

Fig. 9. Short circuit snake principle.

is to use the detected contour at image $(k-1)$ to initialize the one at image k.

This method has been employed with success during the arcing period [23]. Nevertheless it does not work during the short-circuiting period sketched on Fig. 9. Indeed there is no line of high gradient between the molten metal bridge and the weld pool. As a consequence some points of the snake can either go in the bridge or be lost in the pool. A solution is to force these points on an estimated edge.

In this purpose we defined three zones of interest: two for the pool and one for the bridge. The chain of ideas is:

(1) to follow the weld pool surface and approximate it by a polynomial,

(2) to project the points of the initial bridge contour on the polynomial curve if $y_i \geq y_{pool}(x_i) + \epsilon$ where $y_{pool}(x)$ is the equation of the weld pool surface and ϵ is a safety margin ($\epsilon = 2$ pixels),

(3) to launch the *greedy* algorithm on the bridge with the projected points forced in a tube around the estimated pool surface.

4 Experimental Validation

In this section, our main concern is the experimental validation of the proposed model. This will be made in two steps: firstly, we focus on the fitting of the simulated current and voltage to the measurements; secondly, we aim at checking the ability of the model to give accurate prediction of variables which are not easily accessible. Here, we focus on the droplet volume (or equivalently its surface assuming a revolution symmetry).

4.1 Simulator

4.1.1 Preliminary Results

The state space representation written from equations presented in Section 2 is used in a simulator implemented in the Matlab language. The physical parameters of the welding process are given in table 1. The dynamics of the measured and simulated welding currents and voltages, for $U_{oc} = 22$ V and a wire-feed rate $S = 2$ m/min, are shown on Fig. 10. The curves correspond to a whole period with the creation of a droplet at the end of an electrode followed by the transfer of the metal to the weld pool.

During the arcing period, molten metal is added to the drop at each time step because of the physical law driving the melting rate in (10). We notice on Fig. 10(b) that, in the arc period, the calculated variables present an order of magnitude close to experimental ones on Fig. 10(a). Consequently we can assume that the main influences represented by the three forces acting on the drop are sufficient for modeling this period. Nevertheless the short-circuit

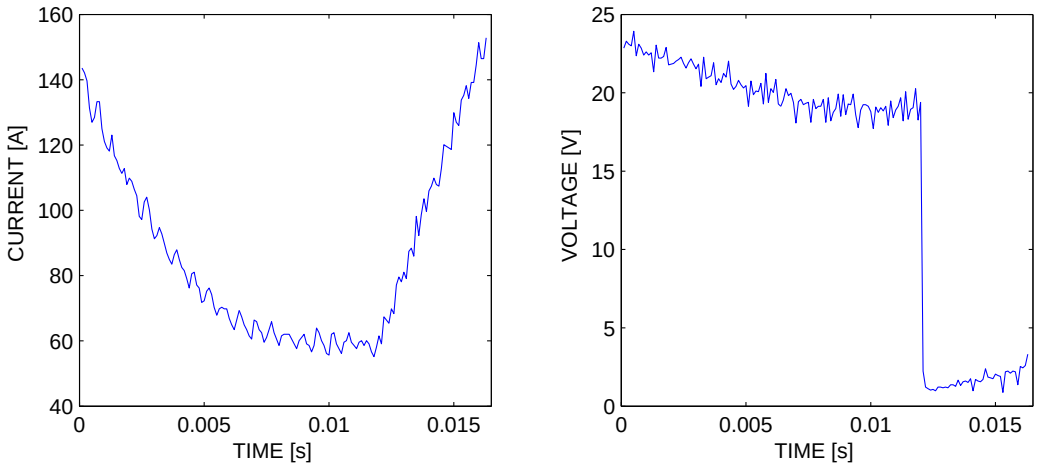

(a)

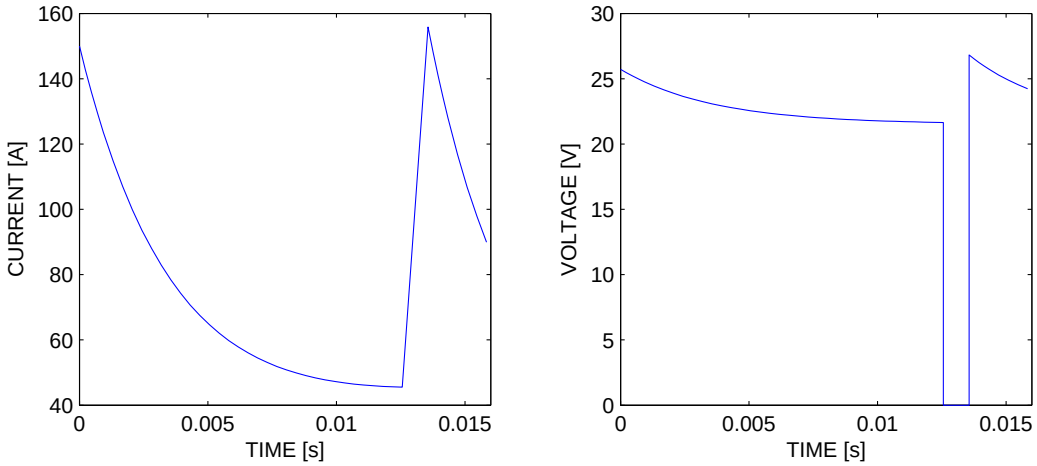

(b)

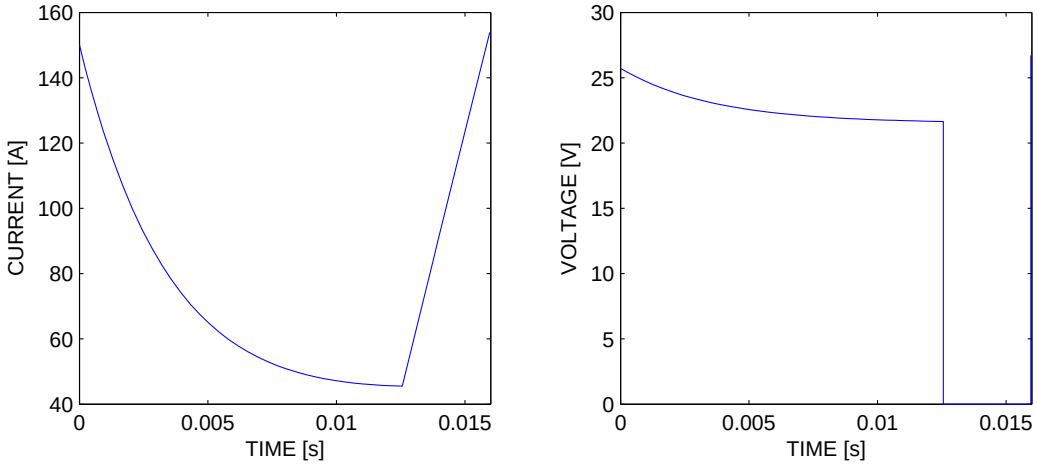

(c)

Fig. 10. Comparison between (a) measured current and voltage; (b) simulated current and voltage; (c) simulated current and voltage with the modified flow expression.

Table 1

List of parameters used for simulation.

Constant	Value
System resistance, R_S	4 mΩ
System inductance, L_S	0.14 mH
Wire radius, r_w	0.5 mm
Linear resistivity, ρ	8.64×10^{-14} Ω/m
Mass density, ρ_w	7800 kg/m^3
Wire feed speed, S	2 or 3 m/min
Contact tip to workpiece distance, CT	15 mm
Permeability, μ_0	1.25×10^{-6} H/m
Surface tension, γ	1.2 N/m
U_0	16 V
R_a	0.036 Ω
E_a	1500 V/m
Arc hanging angle, θ	50^o
Constant for arc heating, C_1	2.96×10^{-14} m^3/As
Constant for Joule heating, C_2	0.0537 m^3/VAs

period seems too short when compared with the experiments. The analysis of the state equations (22)-(26) indicates that the short-circuit duration is

mainly influenced by the current dynamic and the metal flow velocity (21). Recalling that, in fact, the current is controlled during the short-circuit time, so (19) can be modified (through L_S for example) to adjust the simulated current dynamic to experimental data. Also, the derivation of (21) relies on simplifying assumptions which can be questioned. So we propose to modify this equation by introducing a multiplicative factor allowing the simulated current and voltage to be fitted to the experimental ones. The modified expression for the flow velocity is:

$$v = \kappa\sqrt{\frac{2}{\rho_w}(P_{avg} + \rho_w g h)} \tag{36}$$

where κ is an adjustment term. We found experimentally that the values $L_S = 0.7$ mH and $\kappa = 0.25$ yield the results shown on Fig. 10(c). Clearly, the short-circuit duration is now longer and the current dynamic is smaller; they are in better agreement with those observed experimentally in Fig. 10(a).

4.1.2 Adjustment to Experiments

Weld pool oscillation is a dominant feature of short-circuiting welding and a major factor in regards to the welding process stability [24]. The weld pool when excited into motion will exhibit natural frequencies of oscillation [25]. This excitation results from the transfer of the droplet's momentum at the molten bridge rupture [26] and the generation of arc pressure following the ignition of a new arc. According to the authors of [27] the maximal process stability is achieved when the short-circuiting frequency and the oscillation frequency of the weld pool are synchronised such that the short-circuiting frequency equals the oscillation frequency of the pool. Consequently we have chosen to add a motion on the weld pool surface to give a more precise simulation of MIG/MAG welding. The height of molten metal in the pool is

controlled through a function of the type $A\sin(2\pi ft)$. Here we use $A = 1$ mm and $f = 25$ Hz.

4.1.3 Major Tendencies

In this paragraph we want to explain some behaviours of our industrial process thanks to the theoretical equations written previously. We have fixed the wire-feed speed to 3 m/min, the shielding atmosphere and the metal. The changed variable is the open-circuit voltage of the power source. The experimental electrical recordings show that increasing U_{oc} has a great consequence on the length of the arcing period (T_{arc}) and a smaller impact on the length of the short-circuit period (T_{sc}).

On Fig. 11, we have plotted the oscillograms of measured welding voltage and current for $U_{oc} = 22$ V and $U_{oc} = 23$ V. On these short sequences the lowest U_{oc} allows 9 whole periods and the highest one allows 6 periods. By practicing an analysis on a longer sequence, we estimated the averages of T_{arc} and T_{sc} as:

- with $U_{oc} = 22$ V, $\overline{T}_{arc} = 13.75$ ms and $\overline{T}_{sc} = 2.81$ ms,
- with $U_{oc} = 23$ V, $\overline{T}_{arc} = 21.75$ ms and $\overline{T}_{sc} = 3.06$ ms.

Practically speaking, U_{oc} is linked to the so-called *arc length* L_{arc}: when you increase U_{oc} you increase L_{arc}. Arc voltage and arc length are terms that are often used interchangeably. It should be pointed out, however, that they are different even though they are related. Arc length is a critical variable that must be carefully controlled. Should the arc be too long, it tends to wander, affecting both the penetration and surface bead profiles. A long arc

can also disrupt the gas shield. Arc length is the independent variable. Arc voltage depends on the arc length as well as many other variables, such as the electrode dimensions and composition and the shield gas for instance. Arc voltage is an approximate means of stating the physical arc length in electrical terms, although the arc voltage also includes the voltage drop in the electrode extension beyond the contact tube. Welds made with arc voltages that are too low show a depression in the centre of the reinforcement. Arc voltages that are too high create heavy spatter conditions.

Moreover the energy of the arc is higher so the pressure applied on the weld pool surface is stronger. As a consequence the distance between the drop and the weld pool is subjected to an increment when U_{oc} passes from 22 V to 23 V. All these assertions can be checked on Figs. 12(a) and 12(b). A bigger drop has to be created at the end of the electrode. If the distance is increased with a welding current of the same order of magnitude, which means a corresponding melting rate, the time to form this bigger drop is longer.

We can test our simulator and see if this tendency of major significance for an industrial application is well represented. We have used the same parameters and we show on Fig. 13 the oscillograms of simulated welding voltage and current for $U_{oc} = 22$ V and $U_{oc} = 23$ V. On these short sequences the lowest U_{oc} allows 9 whole periods and the highest one allows 7 periods. An analysis made on a longer sequence gives:

- with $U_{oc} = 22$ V, $\overline{T}_{arc} = 22.18$ ms and $\overline{T}_{sc} = 3$ ms,
- with $U_{oc} = 23$ V, $\overline{T}_{arc} = 25$ ms and $\overline{T}_{sc} = 3.05$ ms.

The mean of T_{arc} is increased too by the increment on U_{oc}. This means that our simulator is capable of giving access to information about the frequency

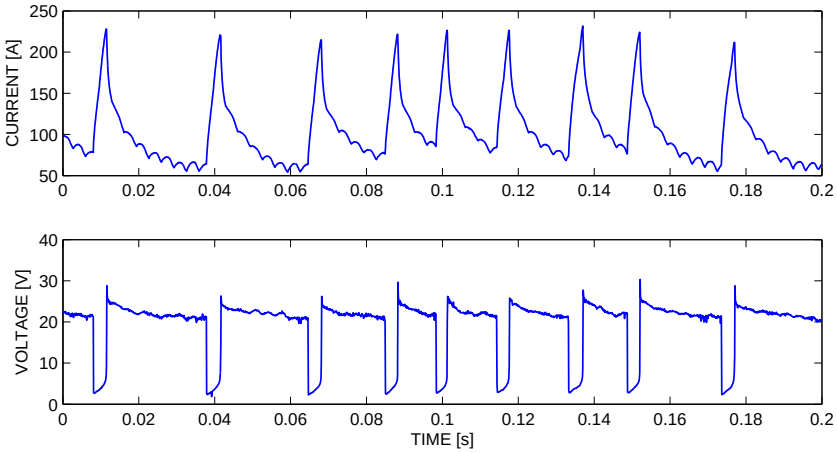

(a)

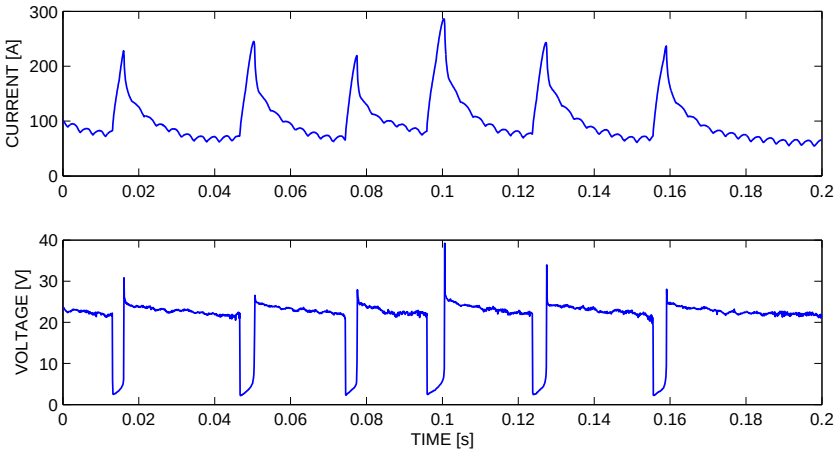

(b)

Fig. 11. Oscillogramms of current and voltage for (a) $U_{oc} = 22$ V, and (b) $U_{oc} = 23$ V.

of the metal transfer phenomenon. This can be of high interest if such an information can be linked to notions of stability or efficiency.

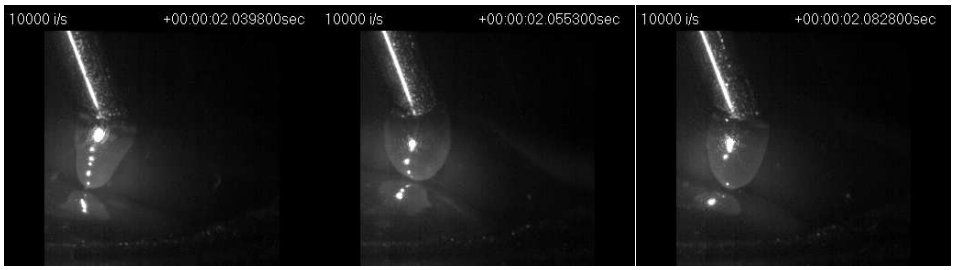

(a)

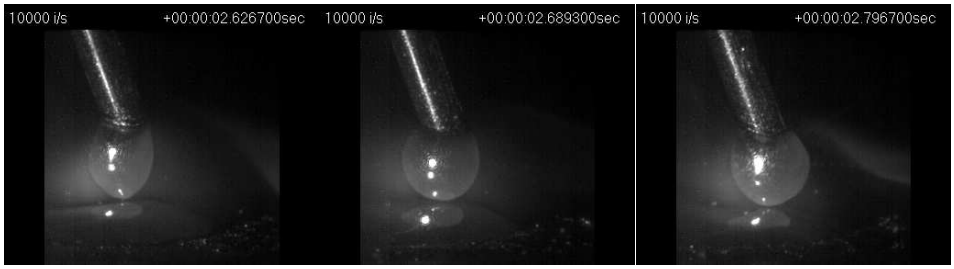

(b)

Fig. 12. Images before short-circuit with $S = 3$ m/min and (a) $U_{oc} = 22$ V; (b) $U_{oc} = 23$ V.

4.2 Active Contours

4.2.1 Preliminary Results

Our experimental data are produced thanks to the method exposed in Section 3. Figs. 14 and 15 are taken from a movie acquired at 10000 frames/sec. We have used a triplet $[1, 1, 1]$ for the active contour in charge of the weld pool surface and a triplet $[0.6, 0.7, 1]$ for the one in charge of the molten bridge. The weight given to the gradient magnitude is increased here because of the lack of luminosity due to the use of an extension tube. The edges are well detected so we will be able to extract the variables of interest for our study, especially the volume of metal included in the drop during the arc period and then the amount transferred to the weld pool during the short-circuit period.

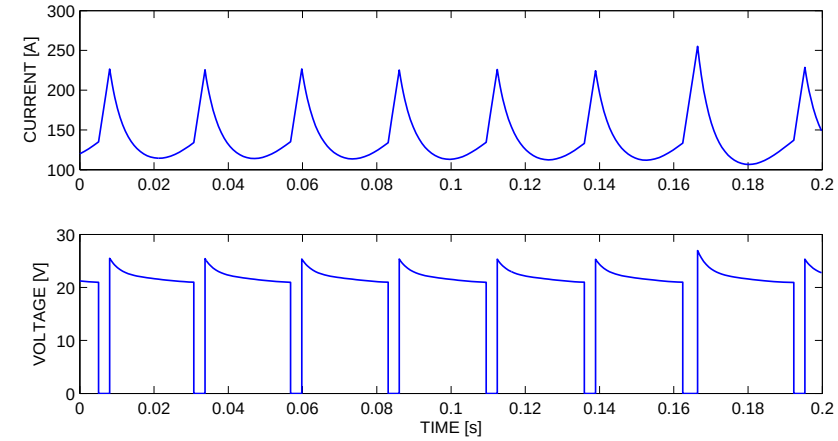

(a)

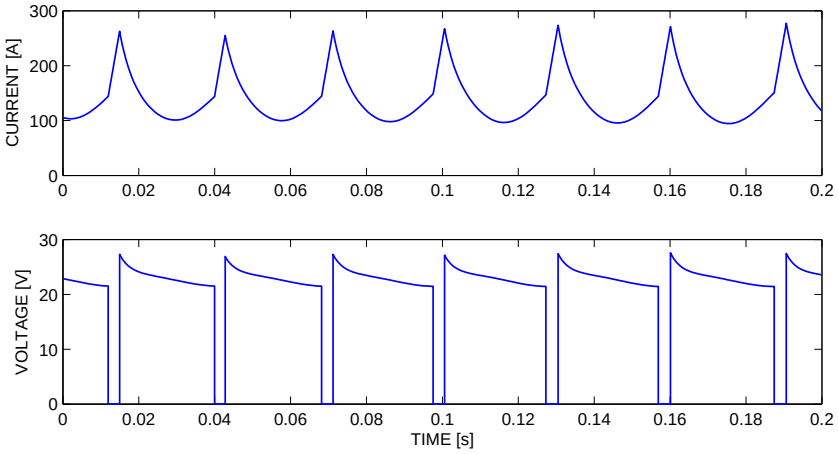

(b)

Fig. 13. Simulated current and voltage for (a) $U_{oc} = 22$ V, and (b) $U_{oc} = 23$ V.

4.2.2 Major Tendencies

On Fig. 16 we have plotted the measured and simulated surfaces of the droplet during the arc period and those of the molten metal bridge during the short-circuit period with an open-circuit voltage $U_{oc} = 22$ V. The measured surface is obtained from the estimated contour of the droplet and then transformed from pixels to millimeters, while the simulated one is computed directly from the geometry of the droplet. We can observe that the surface of the drop at the end of the arc period increases with the open-circuit voltage. This tendency

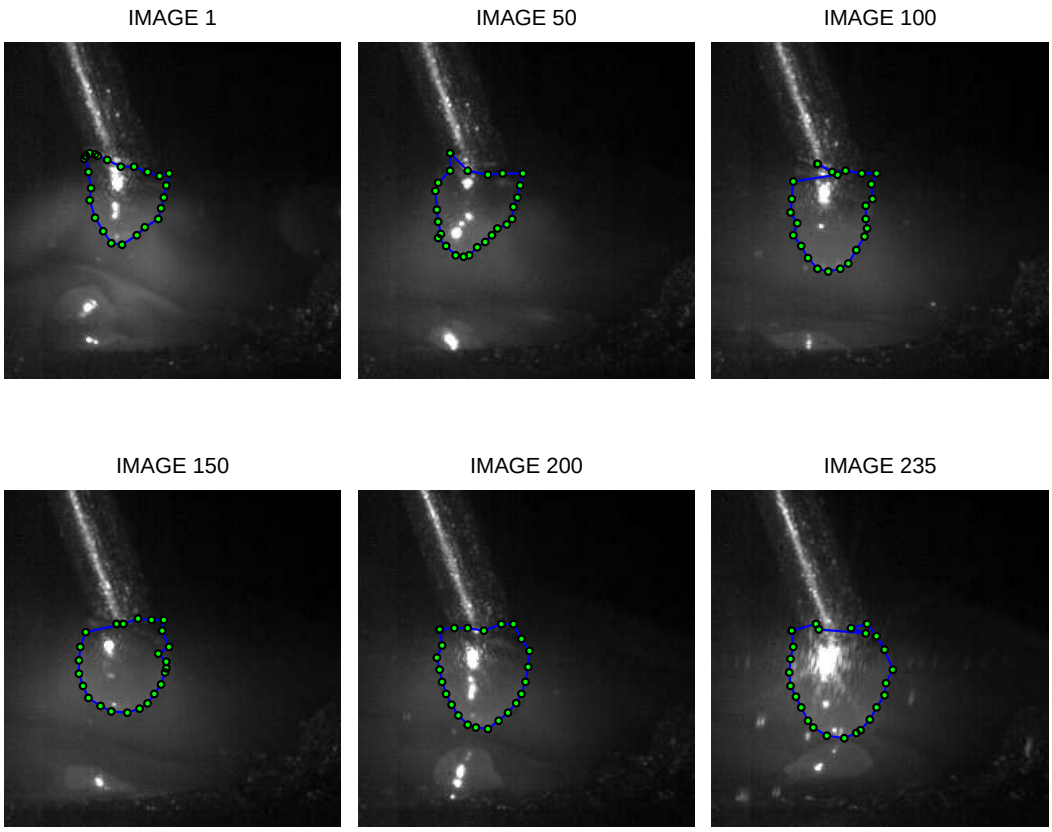

Fig. 14. Converging active contour on a set of experimental images in the arc period.

can be seen on Fig. 17. Indeed, when U_{oc} passes from 22 V to 23 V, the volume of the droplet at the end of the electrode passes from 0.95 mm^3 to 1.45 mm^3. This means that our explanation for the phenomenon observed and simulated is correct: a bigger drop has to be created to allow the physical contact with the weld pool. This has to be used in accordance with the practical knowledge of the welders. The weld diameter at the interface and the reinforcement are the two characteristics of a GMAW weld which determine whether the weld will satisfy the intended service. Two major process variables (weld current and arc voltage) affect one or both of these characteristics. An increase in welding current will result in the following: an increase in the depth and width of the weld penetration; an increase in the deposition rate; an increase in the size of the weld bead. From any specific value of arc voltage, a voltage increase tends

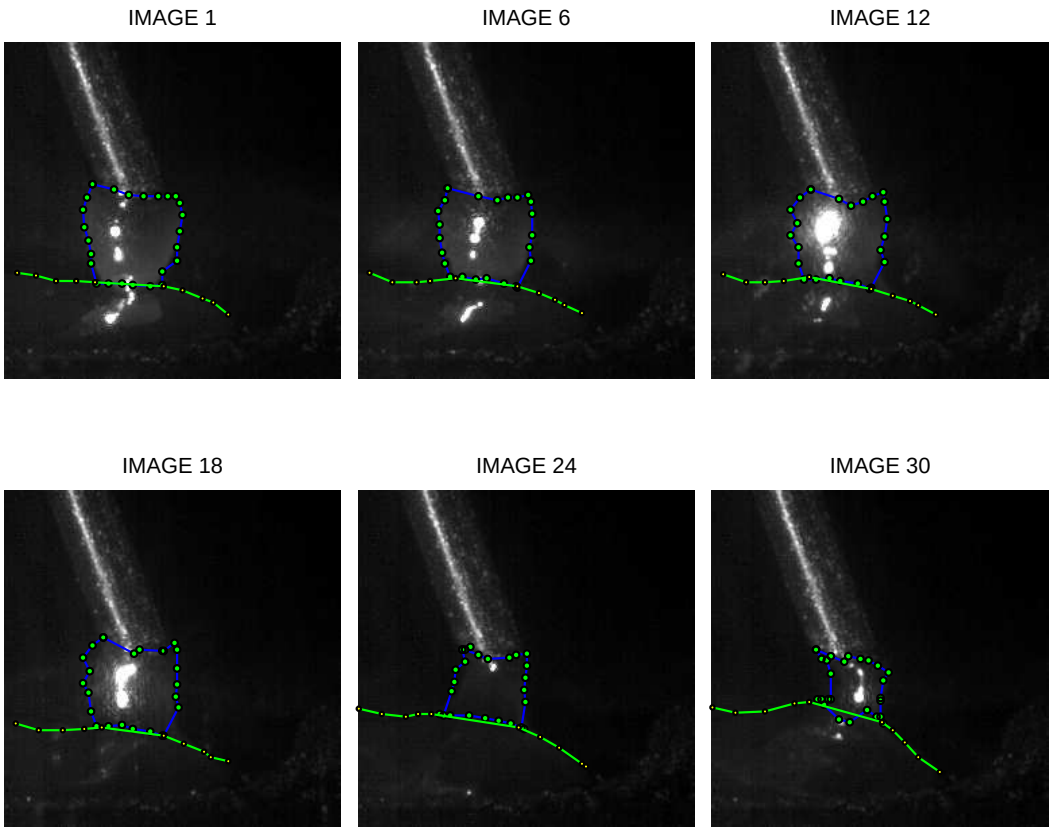

Fig. 15. Converging active contour on a set of experimental images in the short-circuit period.

to flatten the weld bead and increase the width of the fusion zone. Excessively high voltage may cause porosity, spatter and undercut. Reduction in voltage results in a narrower weld bead with a higher crown and deeper penetration. Excessively low voltage may cause stubbing of the electrode.

5 Conclusion

In this paper, we presented the design and testing of a physical model for short-arc MIG/MAG welding. The proposed hybrid model have two distinct continuous states: the arc state during which a drop forms at the end of the electrode, and a short-circuit state when the liquid drop transfers to the weld

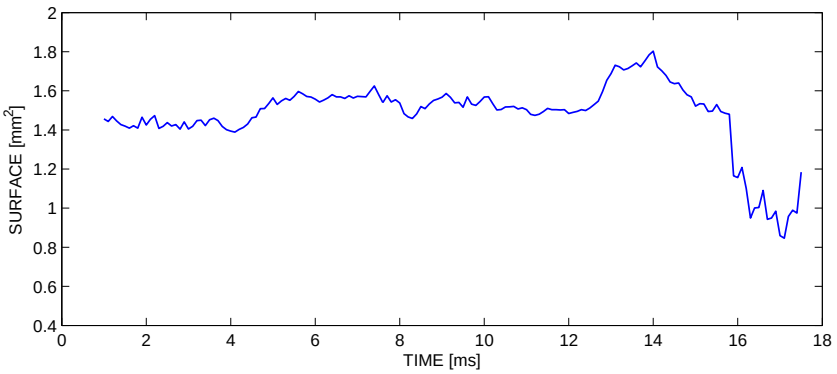

(a)

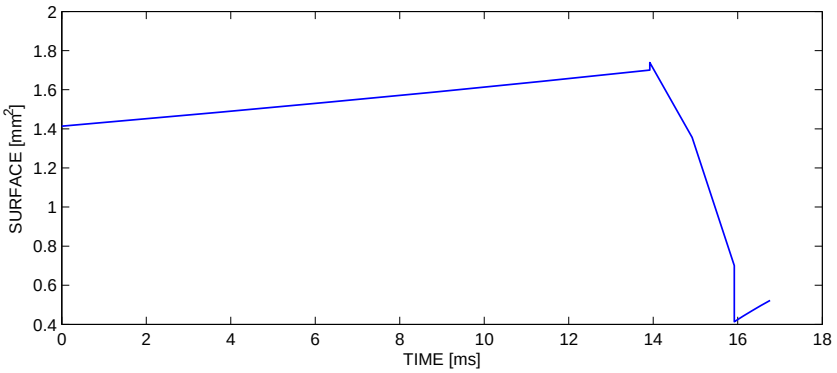

(b)

Fig. 16. Droplet surfaces for $U_{oc} = 22$ V. (a) Measured surface; (b) Simulated surface.

pool. Due to the complex physical interactions involved in the welding process, simplifications have been made to get a model accounting for the main physical contributions. In addition, a discrete contour approach have been developed to follow the dynamical behaviour of the molten drops in image sequences acquired during the welding process. We have shown that model predictions are consistent with experimental data in both arc and short-circuit states. The work will be extended in order to test some control strategies in simulation, and also to help developing fault detection methods in MIG/MAG welding.

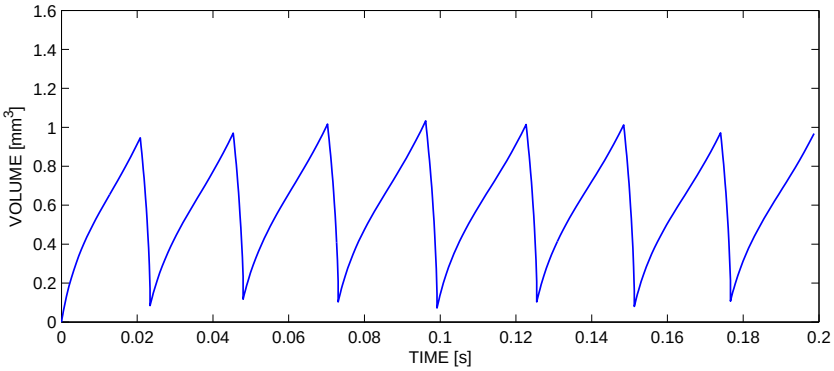

(a)

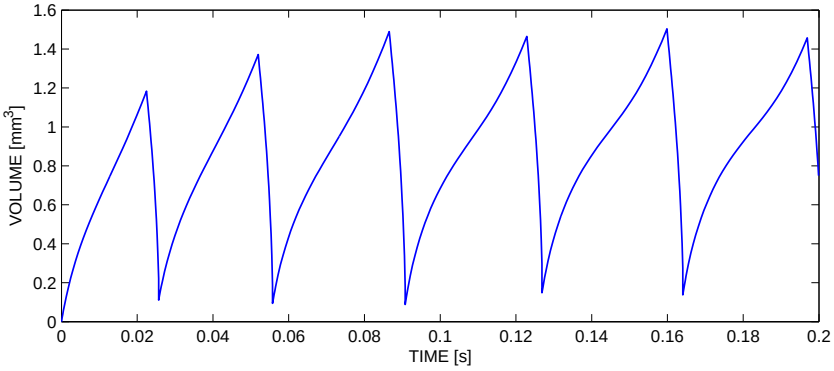

(b)

Fig. 17. Simulated volume for (a) $U_{oc} = 22$, and (b) $U_{oc} = 23$ V.

References

[1] S. Adolfsson, A. Bahrami, G. Bolmsj, I. Claesson, On-line quality monitoring in short-circuit gas metal arc welding, Welding Research Supplement 78 (2) (1999) 59–73.

[2] Y.-S. Kim, Metal transfer in gas metal arc welding, Ph.D. thesis, Massachusetts Institute of Technology (June 1989).

[3] L. Jones, T. Eagar, J. Lang, A dynamic model of drops detaching from a gas metal arc welding electrode, Applied Physics 31 (1998) 107–123.

[4] L. Jones, T. Eagar, J. Lang, Magnetic forces acting on molten drops in gas metal arc welding, Applied Physics 31 (1998) 93–106.

[5] J. C. Amson, Lorentz force in the molten tip of an arc electrode, British Journal of Applied Physics 16 (1965) 1169–1179.

[6] Y.-S. Kim, D. McElliot, T. Eagar, Analyses of electrode heat transfer in gas metal arc welding, Welding Research Supplement (1991) 20–31.

[7] S. Choi, C. Yoo, Y.-S. Kim, Dynamic simulation of metal transfer in GMAW — Part I: Globular and spray transfer modes, Welding Research Supplement (1998) 38–44.

[8] S. Choi, C. Yoo, Y.-S. Kim, Dynamic simulation of metal transfer in GMAW — Part II: Short-circuit transfer mode, Welding Research Supplement (1998) 45–51.

[9] F. Zhu, H. Tsai, S. Marin, P. Wang, A comprehensive model on the transport phenomena during gas metal arc welding process, Progress in Computational Fluid Dynamics 4 (2) (2004) 99–117.

[10] T. Quinn, R. Madigan, T. Siewert, An electrode extension model for gas metal arc welding, Welding Journal 73 (10) (1994) 241–248.

[11] J. Choi, J. Lee, C. Yoo, Simulation of dynamic behavior in a GMAW system, Welding Research Supplement (2001) 239–245.

[12] H. Terasaki, S. Simpson, Circuit simulation for gas metal arc welding system, in: 47th IEEE International Midwest Symposium on Circuits and Systems, 2004, pp. 387–390.

[13] J.-P. Planckaert, E.-H. Djermoune, D. Brie, F. Briand, F.-P. Richard, Modélisation du soudage MIG/MAG en mode short-arc, Tech. rep., Centre de Recherche en Automatique (CRAN) / Centre Technique des Applications du Soudage (CTAS), 35 pages (June 2005).

[14] M. Kass, A. Witkin, D. Terzopoulos, Snakes: Active contour models, International Journal of Computer Vision 55 (1988) 321–331.

[15] W. Harkins, R. Brown, The determination of surface tension (free surface energy), and the weight of falling drops: The surface tension of water and benzene by the capillary height method, J. Am. Chem. Soc. 41 (1919) 499–524.

[16] A. Lesnewich, Control of melting rate and metal transfer in gas-shielded metal-arc welding — Part I: Control of electrode melting rate, Welding Journal 37 (1958) 343s.

[17] H. Delingette, J. Montagnat, Topology and shape constraints on parametric active contours, Report 3880, INRIA, Sophia Antipolis (january 2000).

[18] L. D. Cohen, On active contour models and balloons, Computer Vision, Graphics, and Image Processing: Image Understanding 53 (2) (1991) 211–218.

[19] H. T. Nguyen, M. Worring, R. van den Boomgaard, A. W. M. Smeulders, Tracking nonparameterized object contours in video, IEEE Transactions on Image Processing 11 (9) (2002) 1–11.

[20] D. J. Williams, M. Shah, A fast algorithm for active contours and curvature estimation, Computer Vision, Graphics, and Image Processing: Image Understanding 55 (1) (1992) 14–26.

[21] P. Ladret, B. Latombe, F. Granada, Active contour algorithm: An attractive tool for snow avalanche analysis, Signal Processing 79 (1999) 197–204.

[22] S. Lobregt, M. Viergever, A discrete dynamic contour model, IEEE Transactions on Medical Imaging 14 (1) (1995) 12–24.

[23] J.-P. Planckaert, E.-H. Djermoune, D. Brie, F. Briand, F.-P. Richard, Droplet features extraction with a dynamic active contour for MIG/MAG welding modelling, in: 18th International Conference on Systems Engineering, Coventry, England, 2006, pp. 365–370.

[24] M. Hermans, M. Spikes, G. den Ouden, Characteristics features of the short-circuiting arc welding process, Welding Review International (1993) 80–86.

[25] R. Renwick, R. Richardson, Experimental investigation of GTA weld pool oscillations, Welding Journal 62 (2) (1983) 29–35.

[26] J. Lancaster, Metallurgy of Welding, 5th Edition, Chapman & Hall, London, 1993.

[27] M. Hermans, G. Ouden, Process behavior and stability in short-circuit gas metal arc welding, Welding Journal 78 (4) (1999) 137–141.